Optics Letters

Comparison of the impact of nonlinearity in a *p-i-n* and an MUTC photodetector on electro-optic frequency combs

Seyed Ehsan Jamali Mahabadi,[1,*] **Thomas F. Carruthers,**[1] **Curtis R. Menyuk,**[1] **Jason D. McKinney,**[2] **and Keith J. Williams**[2]

[1]*Computer Science and Electrical Engineering Department, University of Maryland, Baltimore County, Baltimore, Maryland 21250, USA*
[2]*United States Naval Research Laboratory, Washington 20375, USA*
Corresponding author: sjamali1@umbc.edu

We calculate the impact of nonlinearity in both a *p-i-n* photodetector (PD) and a modified uni-traveling carrier (MUTC) PD on an RF-modulated frequency comb generated using 100-fs optical pulses with a 50-MHz repetition rate. We take into account bleaching (nonlinear saturation) that is due to the high peak-to-average-power ratio and contributes to the device nonlinearity. Nonlinear impairment of an RF-modulated continuous wave is typically characterized by the second- and third-order intermodulation distortion products (IMD2 and IMD3). In contrast, an RF-modulated frequency comb must be characterized by a distinct IMD2_n and IMD3_n for each comb line n. We calculate IMD2_n and IMD3_n in both *p-i-n* and MUTC PDs and compare the results. We also calculate the ratio of the IMD2_n power and the IMD3_n power to the fundamental power S_{in} in both *p-i-n* and MUTC PDs. We find that nonlinear distortion has a greater impact at high frequencies in the MUTC PD than in the *p-i-n* PD.   © 2021 Optical Society of America

In this Letter, we theoretically study the impact of nonlinearity in both *p-i-n* and modified uni-traveling carrier (MUTC) photodetectors (PDs) on radio frequency (RF)-modulated frequency combs, and we compare their performance. RF-modulated continuous-wave (CW) optical signals are the mainstay of RF photonics, and the metrics for characterizing nonlinear distortion have been extensively discussed [1]. In contrast, RF-modulated frequency combs have been exploited far less, and the metrics for characterizing nonlinear distortion have not been discussed much. The metrics must be significantly altered since RF modulation produces multiple copies of itself in the frequency domain that surround each comb line.

Frequency combs have important applications in RF photonics. While any CW signal must be limited to powers below the threshold for stimulated Brillouin scattering [2], additional signals outside the gain bandwidth may be launched into an optical fiber without penalty. In principle, an optical comb with N comb lines can transmit N times as much average power through an optical fiber link than is possible in a conventional link that uses a CW source, as long as the comb lines are spaced by more than the Brillouin linewidth and remain with in the PD bandwidth. This idea was used as the basis for a long haul link architecture [3,4]. Frequency combs can also be used in systems that generate low-noise microwave signals [5] and in systems to disambiguate radar signals [6].

Bleaching or absorption saturation is an important issue in RF-photonic systems that use frequency combs. Frequency combs in the RF domain are generated by using a train of short, high-peak-power optical pulses that are converted into a comb in the RF domain by a PD. Typical pulse trains employed in broad bandwidth RF-photonic applications utilize pulses with durations less than 500 fs and repetition rates ranging from 20 MHz to 1 GHz. Hence, the peak power is larger than the average power by a factor $10^4 - 10^6$. The physical origin of bleaching is not well understood at this time. Regardless of its origin, it leads to a decrease in the PD's responsivity. Juodawlkis *et al.* [7] have reported that it can limit the performance of photonic analog-to-digital converters.

We have developed an empirical modeling of bleaching and incorporated this model into one-dimensional (1D) drift-diffusion equations to calculate device responsivity. In preliminary work, we separately described the impact of bleaching on MUTC [8,9] and *p-i-n* [10] PDs. In this work, we compare the impact of nonlinear distortion on these two PDs. The specific PDs that we consider have been previously described [8–10]. For completeness, we give the details of the device design in Supplement 1.

For the PDs that we consider, both the responsivity and bandwidth are larger for the *p-i-n* device. We modified a model that we previously used [11] to include the effect of bleaching. In this model, we defined the optical generation rate in the drift-diffusion equations as

$$G_{\text{opt}} = \beta \, G_c \exp[-\alpha(L - x)], \qquad \textbf{(1)}$$

where β is the bleaching coefficient as a function of the average input optical power, G_{opt} is the optical generation rate, G_c is the generation rate coefficient when bleaching is absent, α is the absorption coefficient, x is distance across the device, and L is

Table 1. Empirical Fitting Parameters in Eq. (2)

Fitting Parameters	MUTC	p-i-n
A	1.0000	1.0000
B	0.0322	0.0098
C	2.7181	0.6526
D	0.1632	0.0236
E	0.0016	0.0015
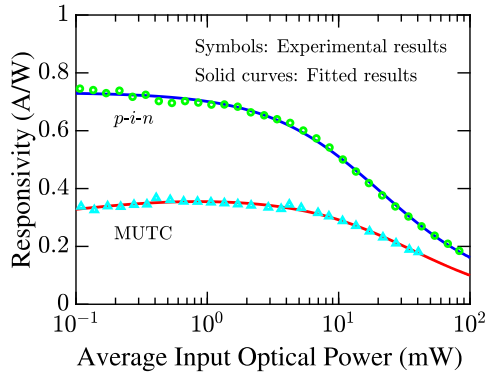
Fig. 1. Responsivity as a function of average input optical power.

the device length. In our model, the parameter β is given by

$$\beta = \frac{A + B I_{\mathrm{p}}}{C + D I_{\mathrm{p}} + E I_{\mathrm{p}}^2}, \qquad (2)$$

where the coefficients A, B, C, D, and E are fit to the experimental data. Table 1 shows these parameters for both p-i-n and MUTC PDs. We have determined these parameters by comparison with experimental results for a p-i-n PD [12] and an MUTC PD [13]. When calculating the parameters of the empirical model, we used a pulse duration of 100 fs for the PD input. This model effectively assumes that the time for the PD to return to the unbleached state is short compared to the repetition time. Figure 1 shows the responsivity of the p-i-n and MUTC PDs as a function of the average input optical power and compares our results to the experimental results in the pulsed mode with a FWHM duration of 100 fs and a repetition frequency of 50 MHz. The experimental setup is described in Refs. [8–10] and is reproduced here in Supplement 1.

We calculate the impact of PD nonlinearity on an RF-photonic signal as a function of the average optical power, including the effect of bleaching. When considering nonlinearity in PDs, the second-order intermodulation distortion (IMD2) and third-order IMD (IMD3) are particularly significant. This is especially true for IMD3, since it generates frequencies that can interfere with the fundamental frequency. The second-order output intercept point (OIP2) and the third-order OIP (OIP3) are the usual figures of merit to characterize IMD2 and IMD3 powers [14]. OIP2 and OIP3 are defined as the extrapolated intercept point of the power of the fundamental frequency and the IMD2 and IMD3 powers, respectively. There are second-order intermodulation terms at frequencies $f_1 \pm f_2$, $f_1 \pm f_3$, and $f_2 \pm f_3$, and third-order intermodulation terms at frequencies $f_1 + f_2 \pm f_3$ and $f_1 - f_2 \pm f_3$, where f_1, f_2, and f_3 are the modulation frequencies.

In our calculation, the input modulated light power $P(t)$ may be expressed as

$$P(t) = P_{\mathrm{opt}}(t)\{1 + m[\sin(2\pi f_1 t) + \sin(2\pi f_2 t) + \sin(2\pi f_3 t)]\}, \qquad (3)$$

where m is modulation depth, and $P_{\mathrm{opt}}(t)$ is the input power of the optical envelope as a function of time, which is defined as

$$P_0(t) = \sum_n A \operatorname{sech}\left(\frac{t - n T_r}{\tau}\right) \qquad (4)$$

in the pulsed mode, where A is the amplitude of input optical power, T_r is the repetition time, and τ is the pulse width. The three frequencies should be close to each other. In our calculations, we used $f_1 = 10$ MHz, $f_2 = 10.5$ MHz, and $f_3 = 9$ MHz. We chose these three frequencies to be close to each other, to fall inside the 50-MHz repetition frequency, and to avoid aliasing.

The use of frequency combs changes the characterization of nonlinearity in a fundamental way. IMD2 and IMD3 and hence OIP2 and OIP3 all become functions of the comb line number n. Instead of one of each of these quantities, as is the case for a modulated CW input, we must determine these quantities for each comb line. Figure 2 schematically illustrates the photodetection of a modulated periodic train of optical pulses, where T_r is the repetition time, and τ is the pulse duration of the optical signal, which then produces a train of modulated electrical pulses, where $\tilde{P}_{\mathrm{opt}}(f)$ is the Fourier transform of $P_{\mathrm{opt}}(t)$, and $S_i(f)$ is the photocurrent spectral density. The periodic train of optical pulses corresponds to equally spaced comb lines in the frequency domain that are spaced by the repetition frequency and centered around zero. The output of the PD is a modulated periodic train of electrical pulses that corresponds to comb lines in the frequency domain that are again separated by the repetition frequency. Figure 2(c) shows the spectrum of the modulated optical intensity profile and the corresponding frequency domain comb lines. The nth comb line, shown by a red arrow, is surrounded by smaller lines at the modulated frequencies $n f_r \pm f_1$, $n f_r \pm f_2$, and $n f_r \pm f_3$, shown by blue arrows. Associated with each comb line is a fundamental power $S_{\mathrm{in}} = S_i(n f_r)$, as well as the power in each of the modulated components.

Figure 2(d) shows the power spectrum of the modulated photocurrent. There is a set of comb lines, indicated by black arrows. Each comb line is surrounded by lines at modulation frequencies $n f_r \pm f_1$, $n f_r \pm f_2$, and $n f_r \pm f_3$, shown by blue arrows, lines at IMD2$_n$ frequencies $n f_r \pm (f_1 - f_2)$, shown by magenta arrows, and lines at IMD3$_n$ frequencies $n f_r \pm (f_1 - f_2 + f_3)$, shown by green arrows. In this figure, we show the fundamental frequency, the modulated frequency components, and the additional IMD2$_n$ and IMD3$_n$ components for each comb line.

We calculate the nonlinearity as a function of the average input optical power $P_{\mathrm{opt}}(t)$, given in Eq. (3), for modulation depth $m = 4\%$. For pulsed inputs, we first calculate the impulse response of the PD for different input optical pulse energies, and we then combine the electrical pulse in the time domain, given by Eq. (4), taking into account the gap of 20 ns between the pulses, to obtain the total electrical response $P_e(t)$ over a long modulation time. We next calculate the Fourier transform of $P_e(t)$ to determine the harmonic powers of the photocurrent for a different choice of the amplitude A. The principal effect of bleaching is to lower the responsivity of the PD so that fewer photocarriers are produced.
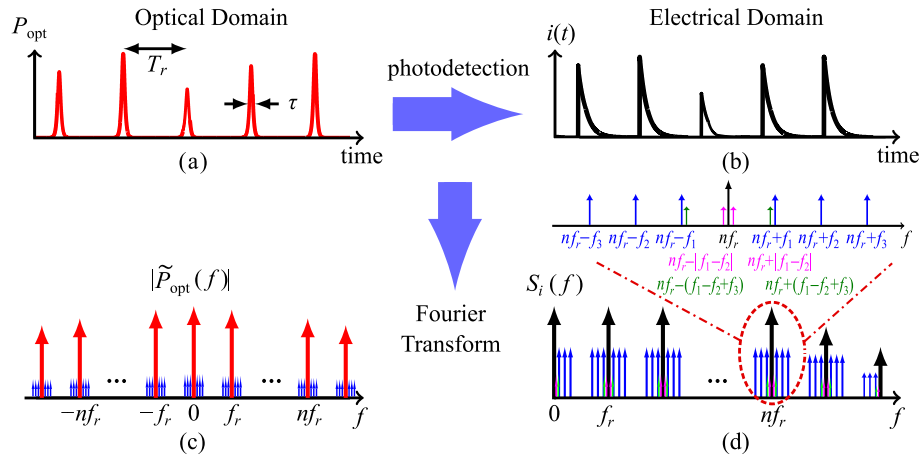
Fig. 2. Time and frequency domain depictions of modulated optical and electrical pulse trains. (a) Modulated optical pulse train intensity profile. (b) Modulated electrical pulse train. (c) Spectrum of the modulated optical intensity profile. (d) Power spectrum of the modulated photocurrent.

Hence, bleaching lowers the power at the fundamental frequencies S_{in}, but also decreases the contribution of space-charge to the nonlinearity. In this work, we focused on the $\mathrm{IMD2}_n$ products at $n f_r + (f_1 - f_2)$ and the $\mathrm{IMD3}_n$ products at $n f_r + (f_1 - f_2 + f_3)$. These are the frequency combinations closest to the fundamental. We calculate one $\mathrm{IMD2}_n$ and one $\mathrm{IMD3}_n$ and from that one $\mathrm{OIP2}_n$ and one $\mathrm{OIP3}_n$ for each comb line n. We calculate $\mathrm{IMD2}_n$, $\mathrm{IMD3}_n$, $\mathrm{OIP2}_n$, and $\mathrm{OIP3}_n$ for a single comb line n as a function of comb line frequency $f = n f_r$, where f_r is the repetition frequency of the input optical power (50 MHz), and compare the results for the p-i-n and MUTC PDs. We also calculate the ratio of $\mathrm{IMD2}_n$ and $\mathrm{IMD3}_n$ to the fundamental power for each comb line n.

Figure 3(a) compares $\mathrm{OIP2}_n$, and Fig. 3(b) compares $\mathrm{OIP3}_n$ for modulation depth $m = 4\%$ in the p-i-n and MUTC PDs. $\mathrm{OIP2}_n$ and $\mathrm{OIP3}_n$ for the p-i-n PD have fallen by ~ 5 dB at 28 GHz, while $\mathrm{OIP2}_n$ and $\mathrm{OIP3}_n$ for the MUTC PD have fallen by more than 20 dB at 18 GHz. As we will discuss shortly, this difference leads to a dramatic difference in the distortion-to-signal ratios. To explain this difference between the p-i-n and
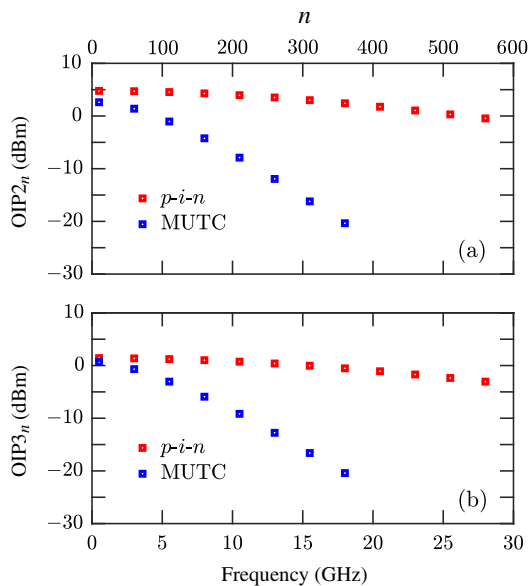
MUTC PDs, we plot the fundamental power, $\mathrm{IMD2}_n$ power, and $\mathrm{IMD3}_n$ power in Fig. 4 as a function of frequency. The blue-square curve, red-square curve, and green-square curve show, respectively, the fundamental, $\mathrm{IMD2}_n$, and $\mathrm{IMD3}_n$ powers for the p-i-n PD. The blue-dotted curve, red-dotted curve, and green-dotted curve show, respectively, the fundamental, $\mathrm{IMD2}_n$, and $\mathrm{IMD3}_n$ powers for the MUTC PD. Some of the differences between these two PDs can be attributed to the differences between the 3-dB bandwidth of the two devices that we considered, which are 29 GHz for the p-i-n PD and 19 GHz for the MUTC PD. However, most of the difference is due to the difference in the $\mathrm{IMD2}_n$ and $\mathrm{IMD3}_n$ powers as a function of frequency. $\mathrm{IMD2}_n$ and $\mathrm{IMD3}_n$ both steadily decrease as the frequency increases for the p-i-n PD. In contrast, $\mathrm{IMD2}_n$ increases for the MUTC PD up to 10 GHz before starting to decrease, while $\mathrm{IMD3}_n$ steadily increases over the entire frequency range.

This increase in the distortion products is somewhat unintuitive, but the distortion products in the frequency comb near a given comb line $n f_r$ is obtained from the combined contribution of many signals, so that, for example, the distortion product $n f_r + (f_1 - f_2)$ will be obtained from many signals at $l f_r + f_1$ and $m f_r - f_2$, where l and m are integers such that $l + m = n$. The distortion products add more coherently in the MUTC PD than they do in the p-i-n PD. We have verified that $\mathrm{IMD2}_n$
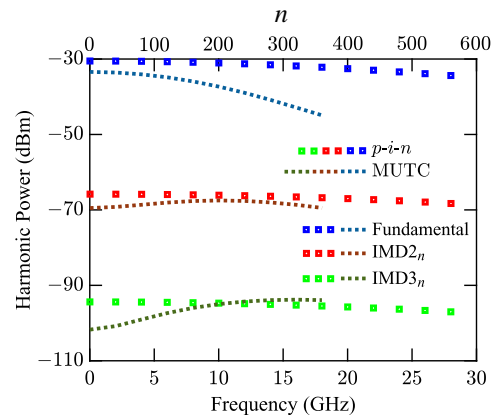

Fig. 3. Comparison of (a) $\mathrm{OIP2}_n$ and (b) $\mathrm{OIP3}_n$.

Fig. 4. (a) Fundamental and (b) $\mathrm{IMD2}_n$ and $\mathrm{IMD3}_n$ powers as a function of frequency in the p-i-n and MUTC PDs.
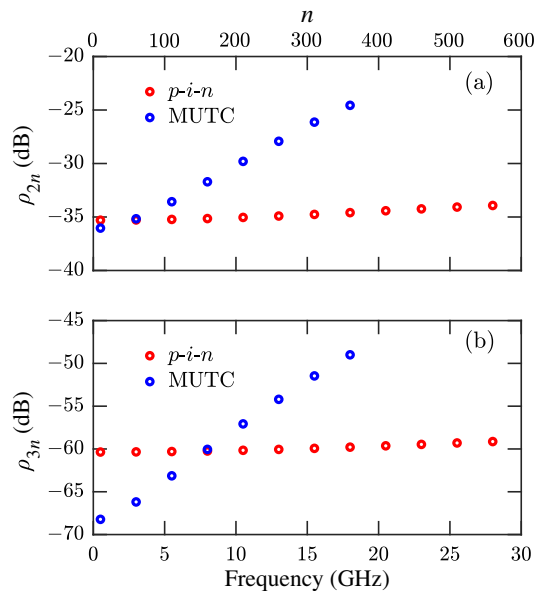
Fig. 5. Distortion-to-signal ratios. (a) ρ_{2n} and (b) ρ_{3n}.

and IMD3$_n$ steadily decline up to 50 GHz for the p-i-n PD, as shown in Fig. S4 of Supplement 1. Hence, this difference in behavior is not due to the difference in the bandwidths of the particular PDs that we considered. The current in the MUTC PD is almost entirely due to electrons, while the current in the p-i-n PD has significant contributions from both electrons and holes flowing in opposite directions. We attribute the lower coherence in the summation of the distortion products at each frequency to the presence of two carriers. We will discuss the individual contributions of each carrier in more detail elsewhere. We have verified that this key result remains unchanged when we increase the modulation depth to $m = 8\%$, as we will discuss in more detail elsewhere.

In Fig. 5, we show the distortion-to-signal ratios, $\rho_{2n} = \text{IMD2}_n/S_{\text{in}}$ and $\rho_{3n} = \text{IMD3}_n/S_{\text{in}}$. We observe that ρ_{2n} and ρ_{3n} increase rapidly for the MUTC PD, while they remain relatively flat for the p-i-n PD. We find that ρ_{2n} is smaller for the p-i-n PD beyond 2 GHz ($n = 40$), while ρ_{3n} is smaller for the p-i-n PD beyond 8 GHz ($n = 160$). The third-order intermodulation products are particularly important because these products can introduce spurious signals that cannot be filtered out from the fundamental response. This is important for RF-photonic applications where these would appear as false signals of interest. We conclude that nonlinear distortion has less impact at low frequencies in the MUTC PD than it does in the p-i-n PD, but the opposite is true at higher frequencies.

We have developed an empirical model of bleaching based on experimental data that were collected at the Naval Research Laboratory, and we incorporated this model into 1D drift-diffusion equations. We then used this model to compare the impact of nonlinear distortion in p-i-n and MUTC PDs on electro-optic frequency combs. In contrast to a CW input for which there is one set of IMD2 and IMD3 powers, each comb line has its own set of IMD2$_n$ and IMD3$_n$ powers. We determined the behavior of the closest-in OIP2$_n$ and OIP3$_n$ as a function of frequency for both p-i-n and MUTC PDs and found that while both OIPs decrease by 20–25 dB for the MUTC PD, they decrease by $\sim$5 dB for the p-i-n PD. We also calculated the distortion-to-signal ratios ρ_{2n} and ρ_{3n}. These grow by $\sim$12 and $\sim$20 dB, respectively, for the MUTC PD, while remaining almost flat for the p-i-n PD. This difference in behavior occurs because IMD2$_n$ and IMD3$_n$ are nearly flat or increase, respectively, as the frequency increases in the MUTC PD, while they decrease in the p-i-n PD. We find that the MUTC PD has lower distortion-to-signal ratios at low frequencies, while the opposite is true at high frequencies. The steady increase in distortion of the MUTC PD as the comb line frequency increases is perhaps surprising in light of their superior linearity relative to p-i-n PDs when operating in CW mode [12,13]. These results underline the importance of designing devices to match the applications.

Disclosures. The authors declare no conflicts of interest.

Supplemental document. See Supplement 1 for supporting content.

REFERENCES

1. V. J. Urick, K. J. Williams, and J. D. McKinney, *Fundamentals of Microwave Photonics* (Wiley, 2015).
2. G. P. Agrawal, *Nonlinear Fiber Optics* (Academic, 1995).
3. J. D. McKinney and V. J. Urick, IEEE Trans. Microw. Theory Tech. **59**, 3249 (2011).
4. M. S. Alshaykh, Y. Xuan, D. E. Leaird, J. D. McKinney, M. Qi, and A. M. Weiner, J. Lightwave Technol. **37**, 5773 (2019).
5. J. Millo, R. Boudot, M. Lours, P. Y. Bourgeois, A. N. Luiten, Y. Le Coq, Y. Kersalé, and G. Santarelli, Opt. Lett. **34**, 3707 (2009).
6. S. R. Harmon and J. D. McKinney, Opt. Express **22**, 23928 (2014).
7. P. W. Juodawlkis, F. J. O'Donnell, J. J. Hargreaves, D. C. Oakley, A. Napoleone, S. H. Groves, L. J. Molvar, K. M. Mahoney, L. J. Missaggia, J. P. Donnelly, R. C. Williamson, and J. C. Twichell, in *15th Annual Meeting of the IEEE Lasers and Electro Optics Society (LEOS)* (2002), Vol. **2**, pp. 426–427.
8. S. E. Jamali Mahabadi, T. F. Carruthers, C. R. Menyuk, M. N. Hutchinson, J. D. McKinney, and K. J. Williams, in *IEEE International Topical Meeting on Microwave Photonics (MWP)* (2019), pp. 1–4.
9. S. E. Jamali Mahabadi, T. F. Carruthers, C. R. Menyuk, M. N. Hutchinson, J. D. McKinney, and K. J. Williams, in *IEEE Photonics Conference (IPC)* (2019), pp. 1–2.
10. S. E. Jamali Mahabadi, T. F. Carruthers, C. R. Menyuk, J. D. McKinney, and K. J. Williams, in *IEEE Photonics Society Summer Topical Meeting Series (SUM)* (2020), pp. 1–2.
11. S. E. Jamali Mahabadi, S. Wang, T. F. Carruthers, C. R. Menyuk, F. J. Quinlan, M. N. Hutchinson, J. D. McKinney, and K. J. Williams, Opt. Express **27**, 3717 (2019).
12. K. J. Williams, R. D. Esman, and M. Dagenais, J. Lightwave Technol. **14**, 84 (1996).
13. Z. Li, H. Pan, H. Chen, A. Beling, and J. C. Campbell, IEEE J. Quantum Electron. **46**, 626 (2010).
14. D. M. Pozar, *Microwave Engineering* (Wiley, 2012), pp. 496–523.

Optics Letters

Comparison of the impact of nonlinearity in a *p-i-n* and an MUTC photodetector on electro-optic frequency combs: supplement

Seyed Ehsan Jamali Mahabadi,[1,*] **Thomas F. Carruthers,**[1] **Curtis R. Menyuk,**[1] **Jason D. McKinney,**[2] **and Keith J. Williams**[2]

[1]*Computer Science and Electrical Engineering Department, University of Maryland, Baltimore County, Baltimore, Maryland 21250, USA*
[2]*United States Naval Research Laboratory, Washington 20375, USA*
Corresponding author: sjamali1@umbc.edu

Comparison of the impact of nonlinearity in a p-i-n and an MUTC photodetector on electro-optic frequency combs: supplemental document

In this supplement, we describe the photodetector (PD) structures and simulation parameters that we used in this study. We describe the measurement setup for the experimental data in Fig. 1. We provide simulation results for IMD2$_n$, IMD3$_n$, OIP2$_n$, and OIP3$_n$ up to 50 GHz for the p-i-n PD.

1. PD STRUCTURES

The p-i-n and MUTC PDs that we modeled in this study are the same as the PDs that we studied earlier [1–4].

A. p-i-n PD

In Fig. S1, we show the p-i-n PD structure that we study. It is a single heterojunction device made of InP and InGaAs. The device is composed of a highly-doped transparent n-InP substrate of length $w_n = 0.1$ μm ($N_D = 2 \times 10^{17}$ cm^{-3}), an intrinsic region of n-InGaAs of length $w_i = 0.75$ μm ($N_B = 5 \times 10^{15}$ cm^{-3}), and a degenerately doped p-InGaAs p-region of length $w_p = 1.2$ μm ($N_A = 7 \times 10^{18}$ cm^{-3}), where N_A and N_D denote the acceptor and donor densities, and N_B denotes the unintentional donor density in the intrinsic region. The total length of the photodetector is $L = 2.05$ μm. The incident light is assumed to pass through an aperture on the n-side ohmic contact of the device. The device radius is 15 μm. We modified the length of the intrinsic region from 0.95 μm in the original structure [5] to 0.75 μm in this study to match the responsivity of the structure in our simulations with experimental data that was collected at the Naval Research Laboratory. The simulations were performed with a 5-V bias, and the 3-dB bandwidth of the p-i-n PD is 29 GHz.

B. MUTC PD

Figure S2 shows the MUTC photodetector structure [6] that we use in our model. Green indicates the absorption region, red indicates highly doped InP layers, purple indicates highly-doped InGaAs layers, and white indicates other layers. In each layer, we indicate the material, doping concentration, and thickness. In InGaAsP layers, Q1.1 and Q1.4 stand for quaternary compounds with bandgap wavelengths equal to 1.1 μm and 1.4 μm, respectively. We use n to indicate n-type doping, n^+ to indicate a high n-type doping concentration, p to indicate p-type doping, and p^+ to indicate a high p-type doping concentration. The simulations were performed with a 4-V bias, and the 3-dB bandwidth of the MUTC PD is 19 GHz.
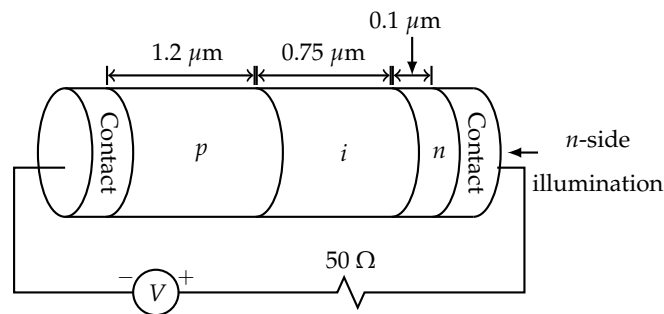

Fig. S1. p-i-n photodetector structure.

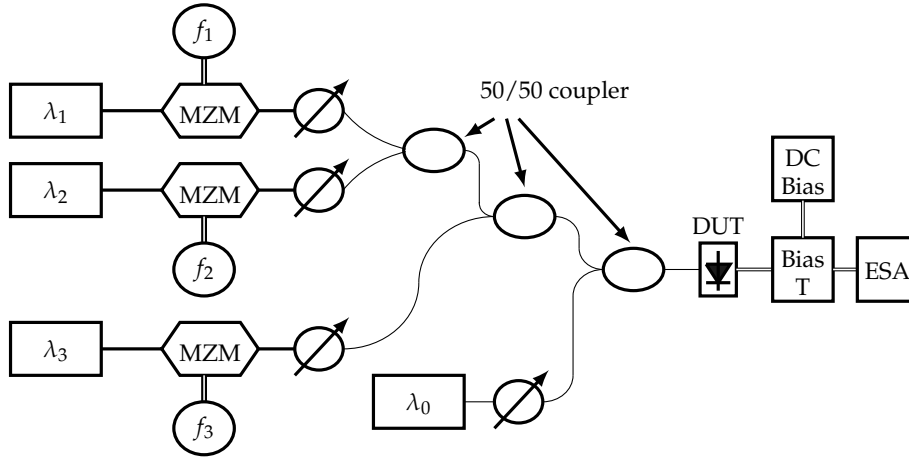**Fig. S2.** Structure of the MUTC PD [6].

Fig. S3. A four-laser three-tone MZM measurement setup. This figure is similar to Fig. 2 in Ref. [7].

2. MEASUREMENT SET UP

Photodetector nonlinearity can be measured using one-, two-, and three-tone measurement systems [7]. Figure S3 shows the setup of a three-tone measurement system. Three Nd:YAG lasers are modulated by three Mach-Zehnder Modulators (MZMs) and their output is fed through optical attenuators. The first two modulated light frequencies are combined using a 50/50 coupler and are then combined with the third frequency using another 50/50 coupler. The unmodulated laser frequency is transmitted through a variable optical attenuator and is then combined with the signal using a final 50/50 coupler. The output is fed into the device under test (DUT). The RF output power is measured with an electrical spectrum analyzer (ESA). The modulation depth is varied by attenuating the lasers.

In the experiments, a Calmar Mendecino passively-modelocked erbium-doped fiber laser was used. The output of the modelocked laser was a train of pulses with a 100-fs FWHM pulse
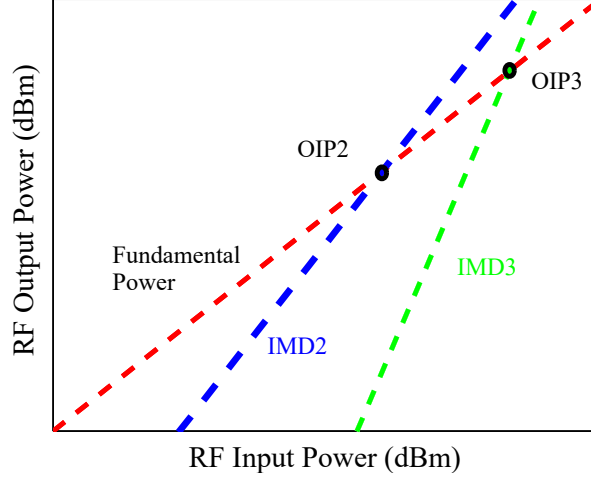
Fig. S4. RF output powers as a function of input optical power.

duration and a 50-MHz repetition rate. The output was passed through a variable attenuator and a calibrated optical tap with a 90/10 splitter. The 10% tap was used as a power monitor and the 90% tap illuminated the PD. The average optical power and average photocurrent were measured as the optical attenuator was adjusted. Knowing the repetition rate, the optical power was then converted to a pulse energy to calculate the responsivity.

3. OUTPUT INTERCEPT POINTS

The second-order output intercept point (OIP2) and third-order output intercept point (OIP3) are defined as the extrapolated intercept point of the power of the fundamental frequency and the second-order intermodulation distortion power (IMD2) and third-order intermodulation distortion power (IMD3), respectively. On a log-log plot, the slope of the fundamental power is 1 and the slope of the IMD2 power is 2, as shown schematically in Fig. S4. OIP2 can be calculated from the fundamental power and the IMD2 power,

$$\text{OIP2} = 2P_f - P_{\text{IMD2}}, \tag{S1}$$

where P_f is the fundamental power in dBm, and P_{IMD2} is the power of the IMD2 in dBm [7, 8]. The slope of the IMD3 power on a log-log plot is 3, and we show it schematically in Fig. S4. OIP3 can be calculated from the fundamental power and the IMD3 power,

$$\text{OIP3} = P_f + \frac{1}{2}\left(P_f - P_{\text{IMD3}}\right), \tag{S2}$$

where P_{IMD3} is the IMD3 power in dBm [7, 8].

4. HARMONIC POWERS AT HIGH FREQUENCIES

Here we present our results of harmonic powers and output intercept points for the *p-i-n* PD up to 50 GHz. Figure S5 shows fundamental power and Fig. S6 shows IMD2$_n$, and IMD3$_n$ powers as a function of frequency in the *p-i-n* PD. As can be seen in Figs. S5 and S6, fundamental, IMD2$_n$, and IMD3$_n$ powers decrease as frequency increases. Hence, the difference in the 3-dB bandwidth between *p-i-n* PD and MUTC PD does not account for the difference in the behavior of OIP$_2$, OIP$_3$, and the distortion-to-signal ratios. Figure S7 shows OIP$_2$, OIP$_3$ as a function of frequency up to 50 GHz in the *p-i-n* PD. As can be seen in this figure, the difference in the OIP$_2$, OIP$_3$ over the range of 50 GHz is ~ 9 dB which is much less than ~ 20 dB difference in the case of the MUTC PD over the range of 19 GHz.
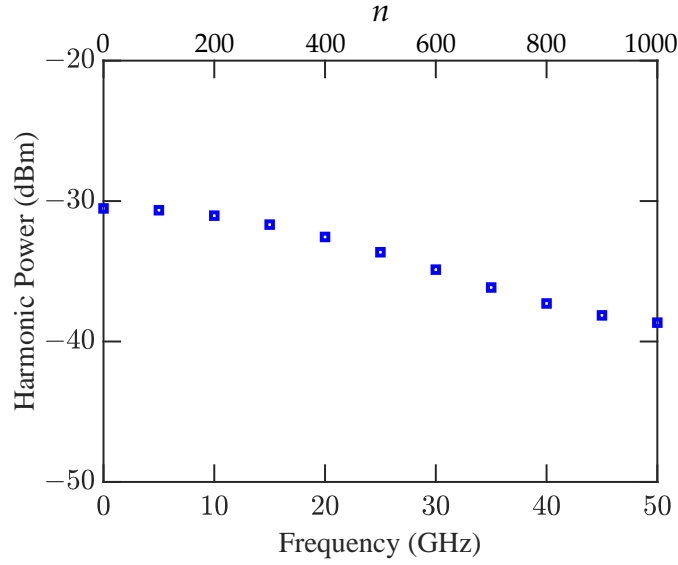
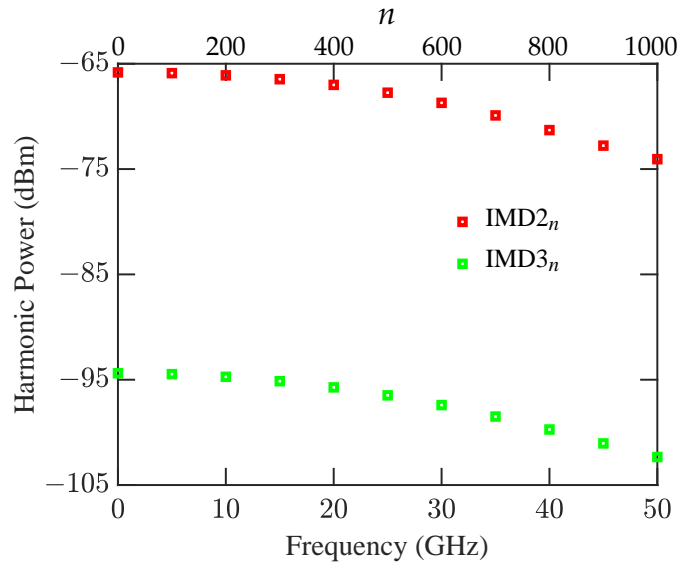**Fig. S5.** Fundamental power as a function of frequency in the *p-i-n* PD.

Fig. S6. IMD2$_n$ and IMD3$_n$ powers as a function of frequency in the *p-i-n* PD.

REFERENCES

1. S. E. Jamali Mahabadi, T. F. Carruthers, C. R. Menyuk, M. N. Hutchinson, J. D. McKinney, and K. J. Williams, "Impact of nonlinearity on RF-modulated frequency combs with different modulation depths in an MUTC photodetector," In IEEE 2019 International Topical Meeting on Microwave Photonics (MWP), 1–4 (2019).
2. S. E. Jamali Mahabadi, T. F. Carruthers, C. R. Menyuk, M. N. Hutchinson, J. D. McKinney, and K. J. Williams, "Impact of nonlinearity in an MUTC photodetector on an RF-modulated frequency comb," 2019 IEEE Photonics Conference (IPC), 1–2 (2019).
3. S. E. Jamali Mahabadi, T. F. Carruthers, C. R. Menyuk, J. D. McKinney, and K. J. Williams, "Impact on frequency combs of nonlinearity including bleaching in *p-i-n* photodetectors," 2020 IEEE Photonics Society Summer Topical Meeting Series (SUM), 1–2 (2020).
4. S. E. Jamali Mahabadi, S. Wang, T. F. Carruthers, C. R. Menyuk, F. J. Quinlan, M. N. Hutchinson, J. D. McKinney, and K. J. Williams, "Calculation of the impulse response and phase noise of a high-current photodetector using the drift-diffusion equations," Opt. Express **27**,
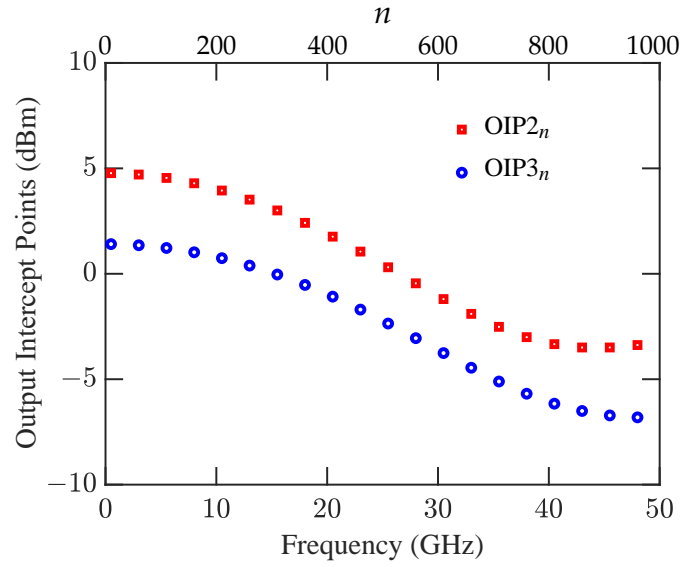
Fig. S7. OIP$_2$ and OIP$_3$ as a function of frequency in the *p-i-n* PD.

3717–3730 (2019).

5. K. J. Williams, R. D. Esman, and M. Dagenais, "Nonlinearities in p-i-n microwave photodetectors," J. Lightw. Technol. **6**, 84–96 (1996).

6. Z. Li, H. Pan, H. Chen, A. Beling, and J. C. Campbell, "High-saturation-current modified uni-traveling-carrier photodiode with cliff layer," IEEE J. Quantum Electron. **46**, 626–632, (2010).

7. M. N. Draa, A. S. Hastings, and K. J. Williams, "Comparison of photodiode nonlinearity measurement systems," Opt. Express **19**, 12635–12645 (2011).

8. D. M. Pozar, *Microwave Engineering* (Wiley, 2012), pp. 496–523.